ADVANCED THERAPEUTICS
www.advtherap.com

Microshell Enhanced Acoustic Adjuvants for Immunotherapy in Glioblastoma

James Wang, Chin-Hsin Huang, Oscar H. Echeagaray, Siamak Amirfakhri, Sarah L. Blair, William C. Trogler, Andrew C. Kummel, and Clark C. Chen**

A key challenge in immunotherapy for glioblastomas, the most common form of primary adult brain cancer, involves the paucity of immune-stimulatory cells in its "cold" immune-microenvironment. Herein, mechanical acoustic ablation focused by perfluorocarbon (PFC) liquid filled silica microshells is applied to induce immunogenicity via in situ ultrasonic lysis. The inert PFC filled ultra-thin walled silica microshells promote mechanical ablation while aiding in ultrasound guidance. In the presence of programmed cell death protein 1 (PD-1) blockade, tumor injury sites exhibit an increase in tumor infiltrating lymphocytes and interferon-γ (IFN-γ) by 1–2 orders of magnitude. At least 75% of mice grafted with the advanced murine glioblastoma tumors achieve remission when treated with a combination of microshell enhanced ablation and PD-1 blockade, which indicates a synergistic effect. In contrast, none of the mice treated with single therapies achieve durable remission. Likelihood of remission correlated with the abundance of tumor infiltrating lymphocytes ($p < 0.001$) and IFN-γ levels ($p = 0.001$). This study demonstrates a PFC filled ultrathin walled microshell enhanced ablation strategy that induces a "hot" immune-microenvironment and augments efficacy of immune checkpoint blockade against advanced tumors.

Glioblastoma is the most common form of adult brain cancer and one of the most aggressive human cancers.[1,2] The median survival of glioblastoma patients after aggressive surgical resection, chemotherapy, and radiation therapy remains ≈14 months.[1] While immunotherapy through checkpoint inhibition has demonstrated impressive clinical efficacy against a number of tumor types,[3,4] its application has been ineffective against glioblastomas.[5] The clinical trial Checkmate 143 exploring the efficacy of the anti-programmed cell death protein 1 (anti-PD1) antibody in recurrent glioblastoma patients showed no therapeutic effect.[6] Subsequent investigations suggest that glioblastoma harbor a "cold" microenvironment, deplete of substrate immune cells required for effective anti-PD1 therapy.[7]

With this understanding, significant interest has emerged to design therapeutic strategies that induce accumulation of requisite immune cells in the glioblastoma microenvironment, thereby transforming a "cold" to a "hot" immune microenvironment. It is hypothesized that modalities affording this transition would augment the therapeutic efficacy of immunotherapies such as checkpoint blockade through anti-PD1 antibodies. Multiple methods have been developed to supplement PD-1 blockade therapies and reach therapeutic efficacy, yet each has certain limitations. Stereotactic radiation combined with PD-1 blockade has been shown to increase the median survival in mice by roughly twofold in glioblastoma but without induced remission.[1] When using nanoscale hafnium (Hf) metal-organic frameworks (nMOFs) as radiation sensitizers,

J. Wang
Department of Nanoengineering
University of California, San Diego
Pacific Hall, Room 4100H, 9500 Gilman Dr. Mail Code 0358, La Jolla, CA 92093, USA
C.-H. Huang
Material Science and Engineering Program
University of California, San Diego
Pacific Hall, Room 4100H, 9500 Gilman Dr. Mail Code 0358, La Jolla, CA 92093, USA
O. H. Echeagaray
Molecular Biology Institute
San Diego State University
500 Campanile Drive, San Diego, CA 92182, USA
Dr. S. Amirfakhri, Prof. S. L. Blair
Moores Cancer Center
University of California, San Diego
3855 Health Sciences Drive, La Jolla, CA 92093, USA
Prof. W. C. Trogler, Prof. A. C. Kummel
Department of Chemistry and Biochemistry
University of California, San Diego
Pacific Hall, Room B100, 9500 Gilman Dr. Mail Code 0358, La Jolla, CA 92093, USA
E-mail: akummel@ucsd.edu
Prof. C. C. Chen
Department of Neurosurgery
University of Minnesota
420 Delaware St SE
Mayo D429, MMC 96, Minneapolis MN 55455, USA
E-mail: cchen@umn.edu
The ORCID identification number(s) for the author(s) of this article can be found under https://doi.org/10.1002/adtp.201900066

DOI: 10.1002/adtp.201900066

 © 2019 WILEY-VCH Verlag GmbH & Co. KGaA, Weinheim

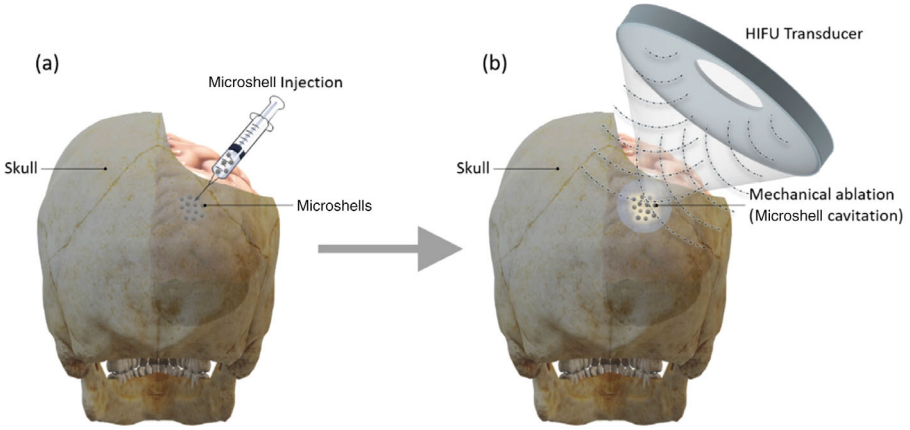

Scheme 1. Proposed therapeutic procedure: a) Microshells are injected into the regions adjacent to the tumor after excision. b) HIFU mechanical ablation is performed on these regions with microshells. Systemic administration of PD-1 checkpoint blockade works synergistically with HIFU induced immune response to establish antitumor activity using the tumor margins. Penetration of the skull would not be necessary since the skull region overlying the tumor will be removed before surgical resection and microshell injection.

radiotherapy combined with PD-1 blockade induced remission on CT26 colon tumors with a 100–150 mm^3 starting volume.[8] Nevertheless, radiation therapy is limited by the maximum X-ray dose that does not cause significant injuries to adjacent tissues or organs.[8,9] Photodynamic therapies with nanomaterials have also been combined with PD-1 blockade as potential treatment methods in breast and colorectal cancer models.[10] However, photodynamic therapy depends on the penetration depth of infrared lasers which varies with tissue type.[11] Additionally, radiation or photodynamic therapies carry the potential for ablating the required immune cell mediator or cross-linking antigens thereby diminishing their immunogenicity. For glioblastoma, an ideal adjuvant therapy to PD-1 blockade treatment should be safe and able to reach deeper tissue structures while participating in the cellular mechanics of immunity re-stimulation. In addition to unique drug and nanoparticle adjuvant combinations,[3,12] one such modality is acoustic based methods such as high intensity focused ultrasound (HIFU).[13] Focused ultrasound based therapies have been demonstrated as a safe, noninvasive therapy for tumors deep in the body.[13] Since ultrasound energy is only focused at the focal point, tissue structures in the beam path are not affected, which results in a noninvasive ablation method with high penetration depth. Unlike other types of ablation methods such as RF, microwave, and laser ablation, HIFU is the only method that is noninvasive.[14] Currently already used in clinical practice, thermal based HIFU has been used to treat uterine fibroids as well as kidney and brain tumors.[14] However, thermal based HIFU can result in thermal stress at tissue locations adjacent to the focal zone due to heat diffusion and lead to potential cellular apoptosis.[15] In contrast, mechanical HIFU is used to generate nonthermal effects that result in lesions with sharp borders of less than 200 µm.[14] Nevertheless, there are unique challenges associated with HIFU as an immune-adjuvant technology. Heat generation from thermal HIFU[14] may compromise immune cell functions[16,17] or trigger denaturation of the proteins required for tumor antigen presentation.[16,17] This consideration is largely addressed by employing low-duty cycle mechanical HIFU, which minimizes heat generation. Low duty cycle HIFU induces subcellular fragmentation resulting in ablative wounds that acts as a reservoir with highly concentrated populations of infiltrating dendritic cells.[14] Previous studies have shown that low-duty cycle mechanical HIFU is more effective in stimulating immunological responses in melanoma and colon adenocarcinoma models relative to thermal HIFU.[16] While checkpoint blockade therapies have been extensively studied and utilized in several cancer types, widespread application is limited by dose-dependent adverse effects; therefore, physical, nondrug adjuvants such as mechanical HIFU are an attractive method to enhance the efficacy of a check point inhibitor without increasing drug burden.

The present study examines the mechanism and efficacy of mechanical HIFU in combination with silica microshells loaded with perfluorocarbon (PFC) liquid to induce accumulation of immune-stimulatory cells within the tumor microenvironment and enhance the efficacy of anti-PD-1 therapy against advanced large glioblastoma tumors.[18] Since glioblastoma is a fast growing tumor where treatment usually begins with surgical resection,[18] large advanced glioblastoma mouse tumor models most closely resemble clinical conditions. In addition, the large size allows the therapy to be tested on highly heterogenous tumors, which is a more stringent test than in most animal studies. The microshells provide a secondary application for image-guided ablation of solid tumors due to the presence of PFC, which is an inert, volatile compound commonly used in food and drug administration (FDA) approved ultrasound contrast agents as an acoustic reflector.[19] These microshells were engineered to undergo inertial cavitation upon interaction with ultrasound and thereby augment cellular lysis and antigen release.[14] Because glioblastoma is aggressively infiltrative, it is expected that microscopic disease remains in regions adjacent to the tumor after excision and is mainly responsible for tumor recurrence.[20–22] An advanced subcutaneous model is used to approximate these microscopic remains after tumor resection. Note that a large opening in the skull is present in standard glioblastoma resection. In this context, it is proposed to directly inject the microshells into these adjacent regions, followed by focused ultrasound application (**Scheme 1**) and systemic checkpoint blockade therapy to establish in situ vaccination against

© 2019 WILEY-VCH Verlag GmbH & Co. KGaA, Weinheim

glioblastoma tumor formation from these infiltrative disease remains.[22] The paradigm of direct therapeutic delivery at the time of tumor resection is one that is widely adopted in several glioblastoma clinical trials. For example, engineered viruses and chemotherapies have been administered in this manner in several clinical trials (e.g., NCT01985256, NCT02798406, NCT02026271). Moreover, ultrasound is routinely used during surgery for intra-operative imaging since the bone opening easily accommodates the ultrasound probe.[23] It is proposed to build on these established paradigms for the therapeutic application of microshells and mechanical HIFU. Given the mechanical property of the cerebrum, it is anticipated that the microshells will remain at the site of the injection and not further penetrate into the tumor. However, the immune infiltrate that accumulates subsequent to PD-1 blockage and mechanical HIFU are expected to disseminate beyond the sites of microshell injection. It is hypothesized that the dissemination of subsequent immune reaction and related antitumor effects underlie the efficacy observed in the present study.

The effects of mechanical and thermal HIFU approaches were tested using ultra-thin walled silica microshells loaded with PFC liquid. Previous studies have shown that microshells with thinner walls require a lower acoustic threshold for ultrasound cavitation in diagnostic imaging.[24] Herein, this concept is further applied for therapeutic ultrasound ablation (HIFU), where ultrathin walled microshells were used as cavitation sources that enable HIFU at low duty cycle and low acoustic pressure.[25] The microshells provide a source for inertial cavitation via acoustic droplet vaporization (ADV)[26,27] to enhance cellular lysis, tissue damage, tumor antigen release, and participate in converting a cold tumor microenvironment into a hot tumor microenvironment.[14,27] Additionally, the cavitation events manifest as bubble clouds and can be observed with an imaging transducer that provides ultrasound guidance for mechanical ablation.[17,28]

The use of liquid PFC filled silica microshells as an acoustic enhancer for HIFU was quantified by induced temperature response. Silica microshells were synthesized via a template-assisted sol-gel method.[29] Phenyl modified silane groups were introduced as part of the silica precursor to create thinner shells.[24] Based on transmission electron microscopy (TEM) analysis, these monodisperse shells consist of a diameter of 1.5 ± 0.06 µm (Figure S4, Supporting Information). It was hypothesized that since thermal HIFU (tHIFU) results in a temperature rise, then addition of silica microshells would further increase the temperature elevation due to cavitation induced vaporization of the PFC droplets. Microshells were initially vacuumed prior to PFP droplet loading. PFP liquid was incubated with microshells at a concentration of 50 µL per milligram of microshells and then subsequently dispersed in water where the PFP droplets were trapped in the hollow core.

For a water solution without microshells, tHIFU insonation induced a temperature increase of 30 °C. In contrast, water solution with microshell suspension resulted in a temperature rise from 0 to 60 °C followed by a drop to 30 °C (**Figure 1**a) when insonated by tHIFU. The high peak temperature rise is consistent with microshells enhancing tHIFU, while the temperature drop to 30 °C represents complete breakage (exhaustion) of all the microshells after 100 s of tHIFU under these conditions. Similarly, to test mechanical HIFU (mHIFU), the HIFU duty cycle was lowered to 2%, and water solutions with and without microshell suspensions were placed at the mHIFU focal zone. For both samples, only a temperature rise of 7 °C was observed (Figure 1b), demonstrating that while microshells may have enhanced mHIFU efficacy, thermal effects were minimal. Comparatively, current clinical MRI guided intra-cranial ablation methods, such as laser ablation and thermal HIFU, both result in an elevation of temperature by at least 55 °C.[30,31] With the presence of microshells as a carrier for acoustically active PFC paired with low HIFU duty cycle, mechanical ablation was achieved with only a 7 °C temperature rise at the region of interest, which is a factor of six less than clinically accepted methods. A TEM study was performed to evaluate if the tHIFU and mHIFU had fractured the microshells. For both tHIFU and mHIFU, the microshells were insonated for 2 min to reach the final state of the systems. TEM of the microshells before tHIFU or mHIFU show intact spheres (Figure 1c). Conversely, TEM of the microshells after both thermal and mechanical HIFU showed broken spheres, consistent with the HIFU induced inertial cavitation that causes shell fracture and can potentially be used for tissue or cellular lysis (Figure 1d).

It is expected that cavitation from fractured silica shells by mHIFU should be sufficient to induce tissue injury, which would in turn serve as foci for recruitment of immune cells.[14] To determine if microshell assisted mHIFU induces tissue injury, silica microshells filled with liquid PFC were injected into porcine liver ex vivo. A diagnostic imaging transducer placed orthogonal to the HIFU beam path was used to guide the HIFU ablation. Simultaneous B-mode ultrasound imaging and contrast pulse sequencing permitted the microshell cavitation events to be superimposed on anatomical references from B-mode imaging. Tissue or mouse was manually adjusted in space to cover a large area of tumor for ablation (Figure 1e). For the porcine liver, treatment with mHIFU (with a 2% duty cycle) without the addition of PFC-microshells did not cause observable, gross tissue damage after 5 min (Figure 1f). In contrast, with the addition of PFC-microshells, a large region of tissue damage was readily observable after mHIFU treatment (Figure 1g).

To test for in vivo liquid PFC filled microshell assisted mHIFU tissue damage, direct injection within the tumor tissue in an animal model was employed.[32] A direct intratumoral (IT) injection allows for sufficient concentration of 1.5 µm microshells within the tumor volume without the need for intravenous circulation that may restrict particle delivery to the tumors and thus require very large doses. It is also noted that the large tumors employed were likely heterogeneous and therefore not all of the tumor might be equally dosed if systemic injection were employed. To overcome the treatment resistance of heterogenous tumors, multiple microshell injections into the tumor were performed so that an immune response could be generated in all tumor microenvironments. As shown in Figure S1a,b, Supporting Information, by spreading the microshells spatially across the tumors, a better tumor remission response could be achieved, consistent with the multiple injections being able to be effective in a large heterogenous tumor. The GL261 murine glioblastoma cells were injected into the flanks of C57BL/6 mice and grown to large advanced tumors. Once a tumor had grown to about 500 mm^3 in volume, the PFC-microshells were directly injected into six different

© 2019 WILEY-VCH Verlag GmbH & Co. KGaA, Weinheim

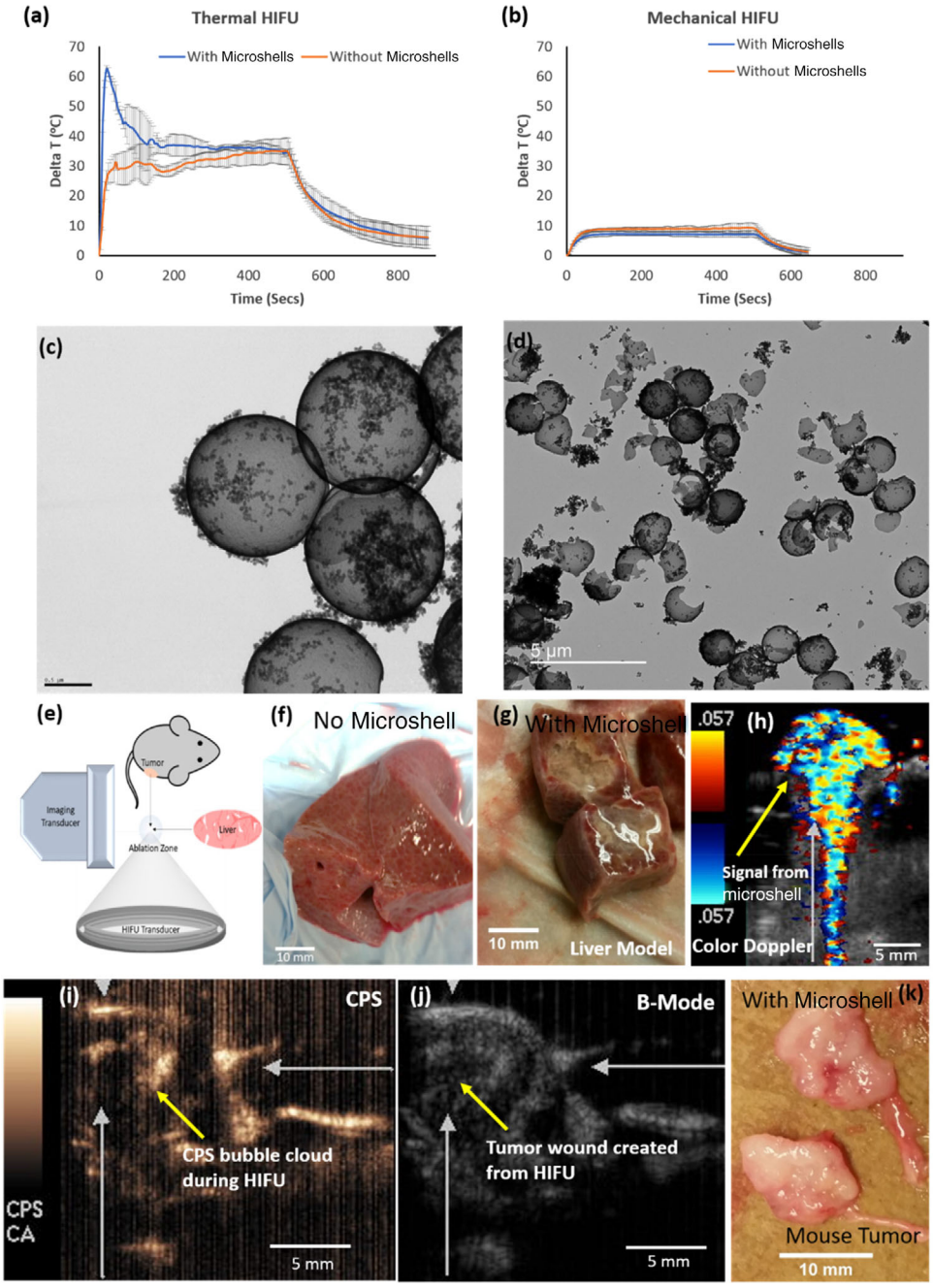

Figure 1. Microshell enhanced HIFU. a) Microshell enhanced thermal HIFU: Microshells induced a maximum 60 °C temperature rise in water compared to a 30 °C temperature rise without microshells. After ≈100 s, the microshells were exhausted resulting in identical temperature profiles. b) Microshell enhanced mechanical HIFU. Microshells induced the same small temperature rise as the solution without microshells in water. c) TEM of microshells before mechanical HIFU. Prior to ultrasonic cavitation, microshells appear intact and can be used to carry PFC liquid, which are strong acoustic reflectors. d) TEM of microshells after 2 min of mechanical HIFU. The mechanical HIFU shattered the microshells due to cavitational shockwaves. e) HIFU schematic detailing imaging transducer used for guiding the orthogonally placed HIFU transducer. f) HIFU without microshells in ex vivo porcine liver. Note that the observed holes are the natural porosity in the liver. g) Microshell enhanced mechanical HIFU resulted in a large tissue ablation area that is visible in the porcine liver when cut open. h) Microshells showing a strong ultrasound color Doppler image for guidance purposes. i) Bubble cloud formation of tumors with microshells enhanced mechanical HIFU visualized by ultrasound imaging. j) Hypoechoic region in B-mode ultrasound of an ablated tumor wound that is visible with ultrasound. k) Microshell enhanced mechanical HIFU in a mouse glioblastoma subcutaneous tumor ($N = 3$), resulting in a liquefied center that was observed after bisection.

© 2019 WILEY-VCH Verlag GmbH & Co. KGaA, Weinheim

locations in each tumor. Six injections spatially distributed in the tumor volume allowed for a more uniform HIFU ablation throughout the tumor environment. Initial studies showed that spatially distributed microshell enhanced HIFU exhibited a more favorable control on tumor size progression compared to single microshell injections (Figure S1a,b, Supporting Information). Because of the echogenicity of PFC, the injection site can be easily imaged by color Doppler imaging (Figure 1h). During mHIFU ablation on mouse flank tumors, bubble clouds were observed during HIFU ablation with contrast pulse sequence imaging (Figure 1i). The bubble clouds were characteristic of cavitation events induced by HIFU exposure. The consequent tissue injury could also be visualized with B-mode ultrasound imaging because the liquefied tissue is hypoechoic and appears as darker regions (Figure 1j). The region of the tissue injury was confirmed after removal of the mHIFU/PFC-microshell treated tumor (Figure 1k). The dark hypoechoic region visualized on B-mode ultrasound imaging. (Figure 1j) corresponded to the anatomic region characterized by liquefied tissue voids (Figure 1k). For subsequent in vivo efficacy studies, these bubble clouds were used as an ultrasound imaging marker to guide the ablation focal zone with an orthogonally placed ultrasound imaging transducer (Figure 1e,j).

Since microshell enhanced mHIFU can result in gross tissue damage without thermal effects, it was hypothesized that in the tumor, such zones of tissue injury can serve as foci for recruitment of immune-stimulatory cells. The lack of temperature elevation would ensure that tumor neo-antigens were not denatured. The relative abundance of T cells in the tumor microenvironment is an important determinant of response to anti-PD1 therapy[33] (**Figure 2**a). CD3 is expressed in all T cells and serve as a general marker for T-cell activity.[34] An immunofluorescence study was performed to determine if mHIFU/PFC-microshell with PD-1 blockade treatment induced the accumulation of CD3+ T cells in vivo (Figure 2b). Mice harboring subcutaneous glioblastoma tumors were treated with mHIFU/PFC-microshell with or without anti-PD1 antibody. While glioblastoma normally occurs in the brain, a subcutaneous model is an essential first step toward developing a protocol for cranial HIFU. With the same tumor models for radiation therapy, therapeutic effects observed in subcutaneous implantation correlates with treatment effects done on orthotopically implanted tumors.[35] Similarly, drug injectables such as dichloroacetate, a kinase inhibitor for inhibiting glioblastoma growth, and micelle loaded paclitaxel have been studied in subcutaneous and intracranial mouse tumors and have shown correlation in tumor suppression between subcutaneous and intracranial tumors.[36] Therapy development that begins with a glioblastoma subcutaneous model allows for ease of tumor access for ablation therapy and frequent monitoring of tumor size, representative of time-sensitive treatment efficacy such as immune therapy. PFC filled microshells were IT injected into mice containing large advanced glioblastoma tumors ($\approx$500 mm^3) in the flank and subjected to mechanical HIFU ablation for 2 min, followed by administration of aPD-1 via intraperitoneal injection (IP) every 2 days for a total of six doses in 10 days. Tumors were harvested at the end of the treatment and analyzed with fluorescence immunohistochemistry (Figure 2c). Initial treatment optimization studies (Figure S1, Supporting Information.) showed that the average tumor growth deflection occurs around day 10 to day 15, which coincides with the end of the treatment schedule (Figure 2c). Consequently, day 10 was used to analyze the tumor-infiltrating immune cells. Rechallenge experiments were employed to determine the long term adaptive immune memory effects. Tissue fluorescent immunohistochemistry analysis showed that multiple foci of CD3+ immunofluorescence was seen only in tumors treated with mHIFU/PFC-microshell combined with anti-PD-1 antibodies (Figure 2b), indicating highly concentrated T cells infiltrating at the tumor site and localized at mHIFU ablation zones. The presence of highly concentrated T cells further confirms that minimizing thermal effects in HIFU tumor ablation can augment the immunostimulatory efficacy of PD-1 blockade.

While CD3 maps the infiltrating T cells in histology sectioning slides, four additional markers for other types of lymphocytes were studied with whole tumor cell population analysis (FACS). The tumor microenvironment was further examined for accumulation of CD45 leukocytes (Figure 2d), CD3 T cells (Figure S2a, Supporting Information), and CD8 cytotoxic T cells (which are considered to be the main effector cells for antitumor response, Figure 2e), CD 4 helper T cells (Figure S2b, Supporting Information) and interferon gamma (IFNγ) expression (Figure 2f). A comparison across all five markers demonstrated a consistent increase in immune activity in the combination cohort when compared to the other groups with monotherapies (mHIFU-NS + Isotype or aPD-1) and control (Figure S7, Supporting Information). CD45 is a receptor that is linked to protein tyrosine phosphatase and is a marker for T-cell activation.[37] CD8 is a membrane protein that is a co-receptor to the T-cell receptor and binds to the major histocompatibility complex (MHC) and is mainly expressed on the surface of cytotoxic T cells. IFNγ is a cytokine that is secreted by the CD8 cytotoxic T cells when acquired immunity develops and is a biomarker used to indicate the activity level of CD8 cytotoxic T cells. Tumor specimens were derived after mHIFU/PFC-microshell/anti-PD1 antibody treatment (or mono-therapies) and analyzed using FACS. For all three biomarkers of immune-activation, significant enhancement was observed when mHIFU/PFC-microshell treatment was performed in combination with aPD-1 treatment (Figure 2d–f). A triple effect was observed. i) The proportion of CD45 leukocytes in the glioblastoma microenvironment was increased more than 20-fold by the combined mHIFU/PFC-microshell/PD-1 blockade treatment relative to each monotherapy (Figure 2d). ii) The proportion of CD8 cytotoxic T-cells in the glioblastoma microenvironment was increased more than 100-fold by the combined mHIFU/PFC-microshell/PD-1 blockade treatment relative to each component treatment (Figure 2e). iii) The expression of IFNγ was increased more than 200-fold after combined mHIFU/PFC-microshell/PD-L1 blockade treatment relative to each component treatment (Figure 2f). These results suggest that mHIFU/PFC microshells facilitated a "cold" to "hot" immune-microenvironment transition when combined with anti-PD1 checkpoint blockade.

A correlation between tumor size and immune response was also observed 10 days after the treatment (Figure 2g–i). For CD45 analysis, smaller tumor sizes after mHIFU/PFC-microshell/anti-PD-1 treatment corresponded to larger populations of tumor infiltrating CD45 cells with a Spearman's correlation coefficient of -0.81($p < 0.001$, Figure 2g). Similarly, tumor size

© 2019 WILEY-VCH Verlag GmbH & Co. KGaA, Weinheim

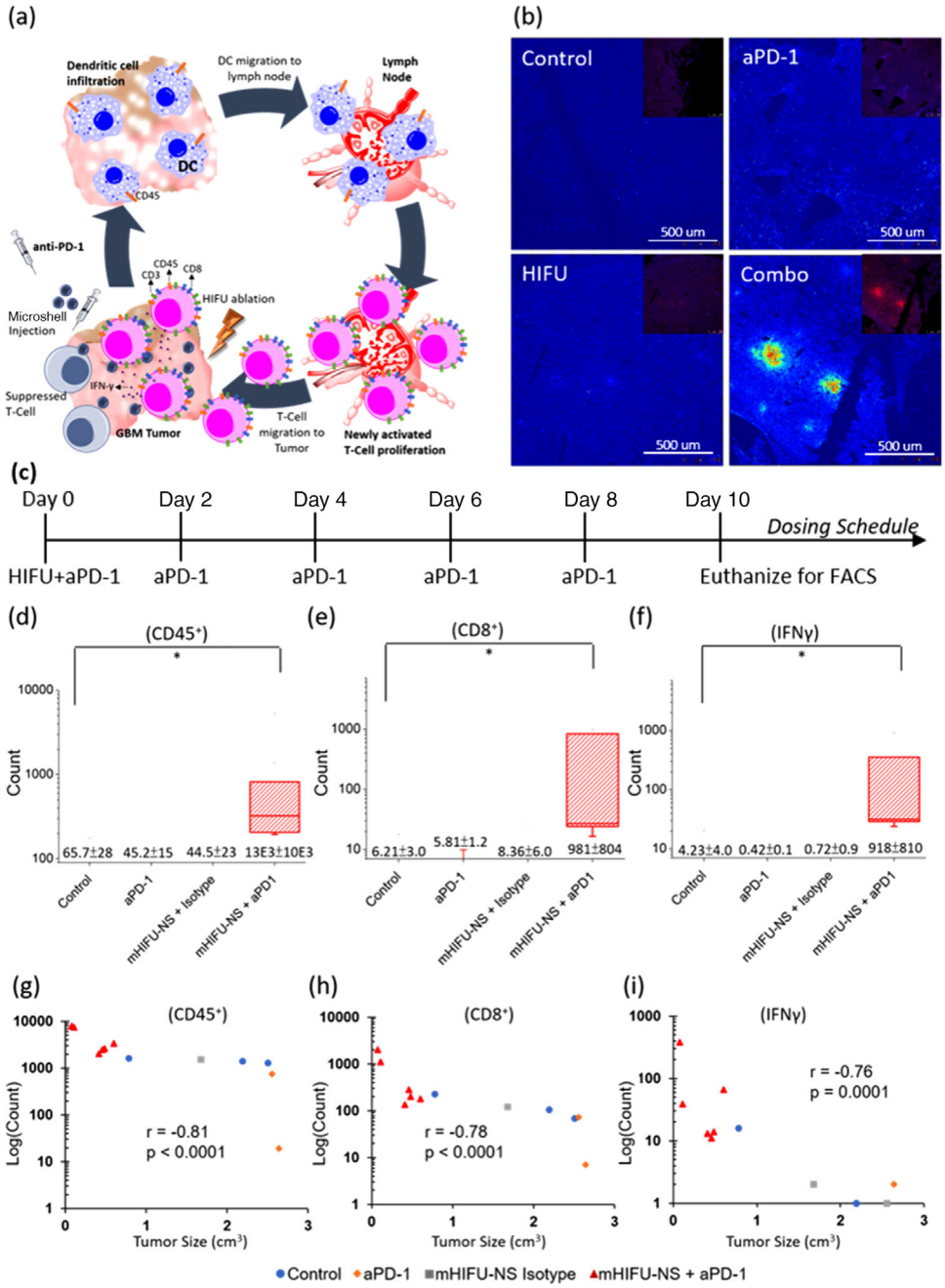

Figure 2. Immunohistochemical analysis. a) Proposed mechanism of acoustic based adjuvants for checkpoint blockade therapies. The GBM tumor is "cold" due to a suppressed immune microenvironment. Mechanical HIFU ablation enhanced by microshells (small blue spheres) are hypothesized to induce in situ cellular lysis via ultrasonic cavitation. The simultaneous PD-1 blockade prevents further immune cell suppression. Dendritic cells subsequently recognize tumor neo-antigens released from cellular lysis and stimulate T-cell proliferation. Newly activated cytotoxic T cells (CD45+, CD3+, CD8+) transform the GBM tumor into a "hot" immune active microenvironment. b) Immunohistofluorescence (IHC) staining of tumor-infiltrating CD3+ T cells and heatmap. Inset is where CD3 T cells are dyed in red while blue is the DAPI nuclear dye. The combination (combo, mHIFU-NS+aPD-1) group shows specific hot spots containing highly concentrated tumor infiltrating T-cells. A heat map was generated for better visualization ($N = 6$). c) Treatment and sample collection schedule. A total of 6 PD-1 blockade doses were administered (one loading dose and five maintaining doses) within 10 days. After the final dose of aPD-1, mice were euthanized for FACS analysis d–f) Box chart showing CD45, CD8, and IFN- γ levels across cohorts ($N = 6$). The mice cohort that received combination therapy of mHIFU-NS with aPD-1 consistently exhibited increased levels of CD45, CD8, and IFN-γ when compared to monotherapies or control groups. g–i) Spearman correlation plots of tumor size versus CD45, CD8, and IFN- γ levels across cohorts showing immune activity that correlates inversely with tumor size. Smaller size tumors showed increased levels of CD45, CD8, and IFN-γ, reflective of antitumor immunity.

© 2019 WILEY-VCH Verlag GmbH & Co. KGaA, Weinheim

inversely correlated with the CD8+ cytotoxic T-cell population (Figure 2h) in the glioblastoma microenvironment, and also IFN-γ ($R^2 = -0.86$, $p = 0.001$, Figure 2i). These results demonstrate that tumor regression after mHIFU/PFC-microshell/anti-PD-1 treatment is largely induced by an activated antitumor host immune response. The association between strong immune activity and small tumor size has also been demonstrated by other groups.[38] Furthermore, increased IFN-γ levels were shown to result in suppressed growth of neuroblastomas.[39] High levels of IFN-γ may induce expression of MHC class I antigens and concomitantly facilitate immune recognition of CD8+ cytotoxic T cells for antitumor activities,[39] consistent with what was observed in the mice cohorts that received mHIFU/PFC-microshell/anti-PD-1 treatments.

A tumor progression study was performed to determine if the transition from that of a "cold" to a "hot" immune-microenvironment induced by the combined mHIFU/PFC-microshell/anti-PD-1 treatment would be associated with enhanced anti-neoplastic effects. PFC-microshells were injected into mice subcutaneously grown with large advanced glioblastoma tumor in the flank (Tumor size of 500 mm^3 on average) and treated with combination or single therapies. Large advanced tumors were employed since they were expected to be the most resistant to immunotherapy treatment and most relevant to clinical settings. With mechanical HIFU or aPD-1 multidose monotherapies, implanted glioblastoma grafts grew at a rate comparable to the control groups (**Figure 3**b–d). In contrast, when microshell enhanced mechanical HIFU was combined with aPD-1, tumor remission was achieved in ≈75% of the implanted glioblastoma grafts (Figure 3e). When thermal HIFU was combined with PFC-microshell and aPD-1 therapies, tumors continued to progress similarly to the control cohort (Figure 3f), suggesting that the thermal effects were associated with tHIFU prohibiting immune-stimulation. The combined survival curves demonstrated that microshell enhanced mechanical HIFU combined with aPD-1 therapies resulted in a significantly improved survival rate of mice with glioblastoma tumors (Figure 3g).

A rechallenge experiment was performed to determine whether acquired immunity against cancer was achieved in the mice. When glioblastoma tumor cells was re-introduced into mice previous implanted and became tumor-free mice after mHIFU/PFC-microshell/aPD-1 treatment, no tumor growth was observed. *These observations suggest that the treated mice had acquired long-term immune memory to glioblastoma when microshell enhanced mechanical HIFU was combined with aPD-1 therapy.*

While immune checkpoint inhibitors have yielded strong clinical efficacy against a number of tumor types,[3,4] application of this strategy to glioblastomas has been challenging.[5] The available data suggest that glioblastoma harbors a "cold" immune microenvironment that lacks requisite immune cells for anti-PD-1efficacy. This work demonstrates the feasibility of converting this "cold" microenvironment to a "hot" micro-environment through mHIFU. When combined with intra-tumoral injection of PFC loaded silica microshell, mHIFU induced inertial cavitation of silica-microshells and caused local tissue damage. While these sites are presumed reservoirs for antigen release and damage associated molecular patterns (DAMPs), the immunosuppressive glioblastoma microenvironment prevents the recruitment of immune-stimulatory cells (i.e., CD45+, CD3+, or CD8+ cells) until anti-PD1 blockade is applied. After PD-1 has been inhibited, dendritic cells that recognize DAMPs and tumor neo-antigens migrate to the lymph node as matured antigen presenting cells (APCs), which stimulate cytotoxic T-cell proliferation with tumor specificity. The newly trained cytotoxic T cells begin to migrate to the tumor microenvironment and are specific to the tumors, while the immunosuppressive PD-1 has been continuously inhibited. Subsequent accumulation of immune-stimulatory cells and IFN-γ expression induced antitumor immunity and led to tumor regression (Figure 2a).

The presence of silica based materials can stimulate an innate immune response via inflammasome activation[40]; in addition, it has been reported that such inflammasome activation was crucial in stimulating a response against dying tumor cells, linking the innate immune pathway with the acquired immune pathway.[41] In the present study, tumor re-challenge experiments suggested that the host had eventually developed acquired immune memory against glioblastoma tumors after combined microshell focused mHIFU and aPD-1 therapy. It is worth considering that the silica material also assisted in developing such acquired immune response.

When administered in combination with the PFC-microshells, mHIFU enhanced the efficacy of anti-PD1 therapy but tHIFU did not. This observation suggests that thermal escalation in the tumor microenvironment compromised the host antitumor immune response. These findings were consistent with previous studies demonstrating that low-duty cycle mHIFU is more effective in stimulating immunological responses than tHIFU in melanoma and colon models.[16] Excessive heat generation may induce protein denaturation or inactivation of cells that compromise antigen presentation and activation of immune response.[16,42] Note that thermal-based HIFU methods have already been developed with magnetic resonance guidance for several brain conditions such as glioblastoma,[43] chronic neuropathic pain, essential tremor, and Parkinson's disease[30] and represents a potential noninvasive ablation method alternative to radiation or surgery in the brain. Furthermore, with the combination of ultrasound microbubbles, HIFU has been used clinically to distrupt blood–brain barriers for more effective drug transport.[30] For the present application, a strategy is proposed whereby the microshells are directly injected into the surgical resection cavity at the time of surgery. Since glioblastoma is aggressively infiltrative, microscopic tumor remains adjacent to the resection cavity can be used to re-stimulate the immune system. Penetration of the skull would not be necessary since the skull overlying the tumor will be removed before surgical resection and microshell injection (Scheme 1). In this context, a subcutaneous tumor model was employed to provide proof-of-principle data for the proposed approach. Furthermore, since human glioblastoma exhibit significant regional heterogeneity in both genotype and phenotype,[21,22] the immune reaction solicited in one region may not be optimal for destruction of tumor in another region. In this context, multiple intra-tumoral injections were performed to spatially distribute the microshells in distinct regions of the tumor, with the goal of soliciting a variety of immune reactions against the inherent glioblastoma heterogeneity. The efficacy observed in the present study supports consideration for clinical translation of this approach.

© 2019 WILEY-VCH Verlag GmbH & Co. KGaA, Weinheim

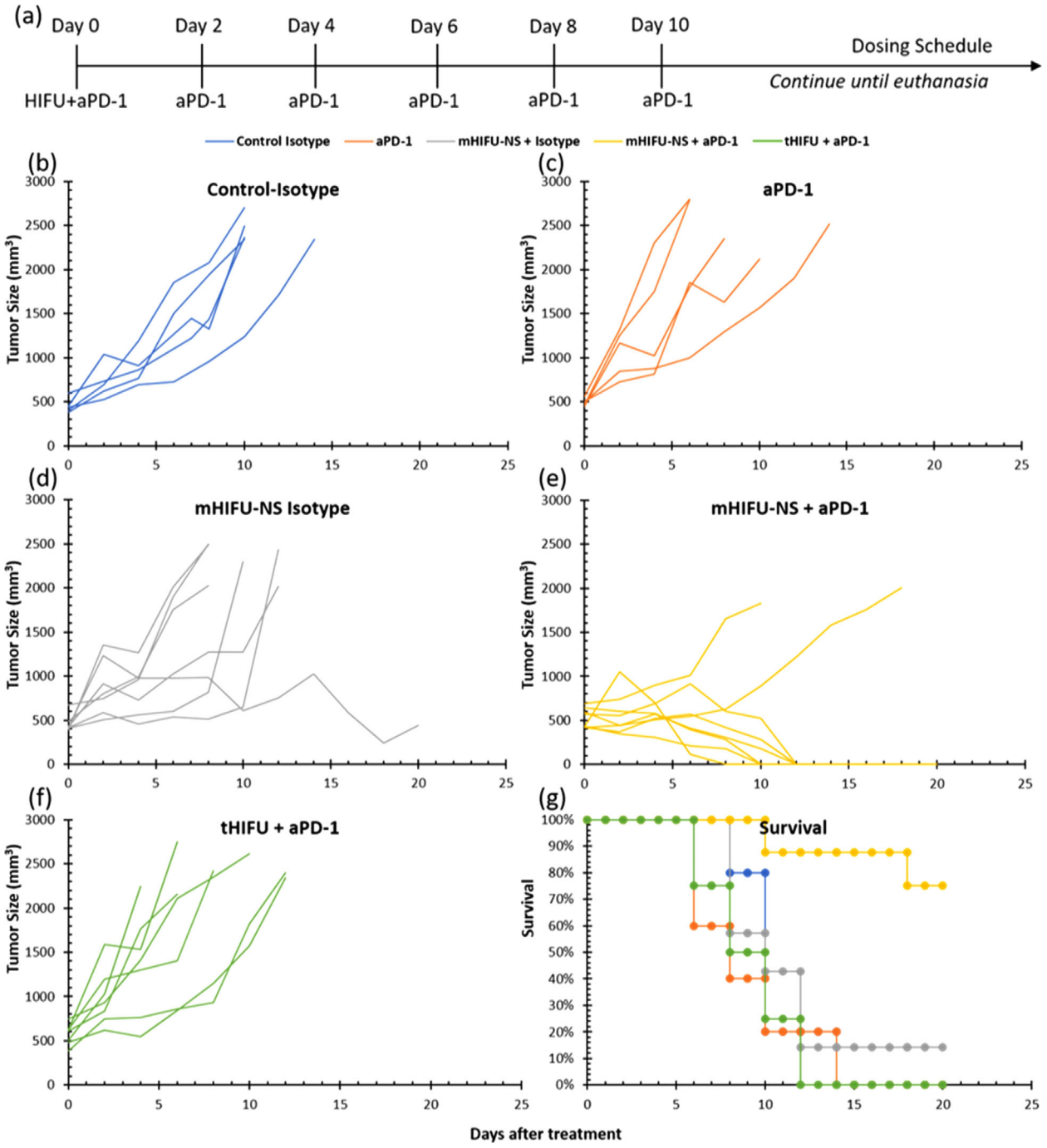

Figure 3. Tumor progression and survival curves. a) Treatment schedule. A total of 6 PD-1 blockade doses was employed (one loading dose and five maintaining dose) immediately after HIFU treatment (Day 0) and lasted for 10 days. b) Individual mouse tumor progression curves for control isotypes. Sample size $N = 5$. c) Individual mouse tumor progression curves for aPD-1 monotherapy. Current PD-1 blockade treatment plan did not result in tumor stabilization, but resulted in tumor growth similar to control cohorts. Sample size $N = 5$. d) Individual mouse tumor progression curves for microshell enhanced mechanical HIFU with isotype monotherapy. Microshell enhanced HIFU resulted in minor level of tumor progression control. Sample size $N = 7$. e) Individual mouse tumor progression curves for microshell enhanced mechanical HIFU with aPD-1 therapy. Microshell enhanced mechanical HIFU combined with PD-1 blockade resulted in 75% of tumor remission. Sample size $N = 8$. f) Individual mouse tumor progression curves for thermal HIFU (tHIFU) with aPD-1 therapy. Tumor progression was similar to control cohorts. Sample size $N = 7$. g) Percent survival after treatment. p-value for tumor size at day 10 was <0.001. Total sample size $N = 32$.

© 2019 WILEY-VCH Verlag GmbH & Co. KGaA, Weinheim

The present study has demonstrated that PFC filled microshells effectively provided a two-pronged approach to complement checkpoint blockade therapies. The presence of inert PFC droplets serves as a cavitation center to promote effective mechanical ablation with minimal thermal effects at low HIFU pressure output while also serving as a source for ultrasound guidance. In the context of PD-1 blockade, the HIFU ablation sites accumulate one to two orders of magnitude of increase in immune stimulatory leukocytes and cytotoxic lymphocytes, thereby converting the immune "cold" glioblastoma microenvironment into a "hot" microenvironment to better facilitate checkpoint blockade treatments. This transition is associated with glioblastoma regression and induction of antitumor immune memory. This work suggest potential new opportunities where physical adjuvants such as acoustic ablation, that participate in immune pathway stimulation, can be tuned to combine with existing immunotherapies for cancer types that are not readily responsive to checkpoint blockade treatments.

Experimental Section

Materials: Tetraorthosilicate (TMOS), *N*-(3-trimethoxysilylpropyl) diethylenetriamine, and trimethyl borate were purchased from Sigma-Aldrich (St. Louis, MO). Polystyrene microbeads were acquired from Polysciences (Warrington, PA). Anti PD-1 antibodies (clone RPM1-14) were obtained from BioXCell (West Lebanon, NH). Perfluoropentane was purchased from Strem Chemicals (Newburyport, MA). Mili-Q purified water was acquired from Milipore SuperQ Plus Water Purification System (Billerica, MA). The microshells used in this study were synthesized with methods previously developed.[17] RPMI Medium 1640 (Gibco, 11875-093) was supplemented with 10% fetal bovine serum (Corning 35-011-CV) and 100 U mL^{-1} penicillin, 100 µg mL^{-1} Streptomycin, 292 µg mL^{-1} Glutamine (Life Technologies, 10378-016, Carlsbad, CA) to prepare complete medium RPMI-10 (RP10).

Microshell Synthesis: Polystyrene templates with a 2 µm diameter were initially suspended in 500 mL of ethanol at a concentration of 5% v/v. DETA at a concentration of 0.2% v/v in 40 mL of ethanol was added into the mixture and stirred at 4000 rpm for 1 h. TMOS (0.19% v/v) and TMPS (0.13% v/v) were added into the mixture and the sol-gel reaction continued in room temperature for 7.5 h at 4000 rpm stir rate. At the end of the reaction, the core shell silica particles were centrifuged at 3200 rpm for 10 min and washed with ethanol five times. After the ethanol washes, the core shell silica particles were air-dried overnight and calcined at 550 °C for a total of 5 h with a 1.5 °C per minute heating and cooling ramp before and after 550 °C. The calcined silica microshells were suspended in ethanol at a concentration of 8 mg mL^{-1} in a vacuum sealed vial with septa. These microshells were vacuumed overnight to remove the ethanol. PFP at a concentration of 50 µL per milligram of silica microshells were injected into the vial at 0 °C ambient temperature and then subsequently, deionized water was injected into the vial to constitute a silica colloidal mixture of 8 mg mL^{-1}.

HIFU Ablative System: A single element HIFU transducer (Sonic Concepts [Bothell, WA]) was operated at 1.1 MHz. An amplifier (T&C Power Conversion [Rochester, NY]) was used to amplify signals generated by a waveform generator card (National Instruments [Austin, TX]) installed on the main board of a PC. Waveforms with varying duty cycles were programed with the National Instruments proprietary waveform editor program. Waveforms consists of sine waves with a frequency of 1.1 MHz and a duty cycle of 2% for mechanical HIFU and 100% for thermal HIFU. A clinical ultrasound imaging transducer from Siemens was used to guide the HIFU ablation.

Animals and Tumor Model: C57BL/6 mice were purchased from the Jackson Labs through UCSD animal care program (ACP). All experimental methods and animal housing conditions were approved by the Institutional Animal Care and Use Committee (IACUC). GL261 glioblastoma cell lines were cultured and about 10^6 cells were injected subcutaneously into the right flank of each mouse. When the tumors reached 400–700 mm^3, treatment commenced. Tumor dimensions were measured with a digital caliper (VWR [Radnor, PA]) and the volumes were determined with established model $V = W \times W \times H/2$ (W is width and H is height).[44] Mice were anesthetized with isoflurane gas during the experiment and euthanized with carbon dioxide asphyxiation followed by cervical dislocation. Tumors were harvested on day ten after treatment and digested with a mouse tumor dissociation kit (Miltenyi Biotec, Germany) in RPMI 1640 according to the manufacture's protocol. Fixation/permeabilization solution kits (BD Biosciences, San Jose, CA) were used for intracellular staining for IFNγ. Flow cytometry was performed on BD FACSCanto. Mice were anesthetized with isoflurane gas during the experiment and euthanized with carbon dioxide asphyxiation followed by cervical dislocation at the end of experiments. To perform drug injection therapy such as control isotype and anti-PD-1 antibodies, mice under isoflurane anesthesia were injected intraperitoneally with 200 µg of drug (aPD-1 or control isotypes) on the first day, followed by 100 µg every other day for five more doses. To perform HIFU tumor ablation, mice were kept under isoflurane anesthetization with the tumor portion submerged in 37 °C water at the HIFU transducer focal zone. An orthogonally placed imaging transducer was used to monitor the ablation region in the tumor by observing cavitational bubble cloud formation due to the microshells. Each location in the tumor was subjected to HIFU exposure with an average dose of 0.3 s mm^{-3}. After the HIFU procedure, mice were removed from isoflurane anesthesia, dried with a cloth, and kept warm during the recovery period. For combination therapies anti-PD-1 antibodies were immediately injected intraperitoneally after the HIFU procedure with a dosing schedule identical to that of anti-PD-1 antibody monotherapy.

Tumor Analysis: In order to study the active immune response during the treatment, C57BL/6 mice were euthanized 10 days after the start of treatment. Tumors were excised and their volume and weight were measured with a caliper and benchtop balance. Tumor dissociation was performed following the standard protocol in the Miltenyl Biotec's tumor dissociation kit. Briefly, the tumors were cut into small pieces with a surgical scalpel and transferred into gentleMACS C tubes (Miltenyl Biotec) with 2.5 mL of digestion buffer solution containing enzyme D, R, and A (Miltenyl Biotec dissociation kit) in RPMI 1640. The tumors in the gentleMACS C tubes were placed on the gentleMACS dissociator (Miltenyl Biotec) at 37 °C for 40 min. Afterward, 5 mL of cold RP10 was added to the tumors in the gentleMACS C tubes and centrifuged at 1200 for 5 min. The pellet was suspended in 5 mL of RP10 and filtered through a 100 µm cell strainer. The cells were subsequently stained with DAPI in order to determine the count of live cells. Antibodies specific to CD45 (Cat # 103114), and CD8 (Cat # 48–0081) were mixed with Fc block-BD stain buffer and mixed with the tumor cell samples for surface marker staining. For IFN-γ (Cat# 17–7311), the tumor cells membranes were first permeabilized by a fixing permeabilization buffer (BD Biosciences fixation/permeabilization solution kits) at 4 °C for 30–60 min. After washing with the BD stain buffer, the cells were mixed with IFN-γ antibodies for intracellular staining for 30 min at 4 °C. After staining, cell solutions were washed twice with 200 µL of buffer and resuspended in 200 µL of PBS. After washes, cell sampels were counted with BD FACSCanto to determine the populations of lymphocytes and IFN-γ levels.

Statistical Analysis: All data are presented as mean ± standard deviation. For particle size distribution, a total number of 246 silica shells from five different regions were measured by ImageJ and calculated for mean and standard deviation. For in vivo mice experiments, each experiment was repeated for at least $N = 3$ times. For FACS analysis, multi-variate ANOVA was used to calculate the p-value for significance. For correlation calculations, a Spearman's coefficient test was used to determine the correlation.

Supporting Information

Supporting Information is available from the Wiley Online Library or from the author.

© 2019 WILEY-VCH Verlag GmbH & Co. KGaA, Weinheim

Acknowledgements

The authors acknowledge the T32 Training grant (5T32CA153915-08) from NCI of NIH and the U54 supplementary grant (5U54CA132379-08) from collaboration with SDSU. Support from Viewpoint Medical is also greatly appreciated. C.C.C. was supported by 1RO1NS097649-01, 9R44GM128223-02, the Doris Duke Charitable Foundation Clinical Scientist Development Award, the Sontag Foundation Distinguished Scientist Award, the Kimmel Scholar Award, and BWF 1006774.01.

Conflict of Interest

Sarah Blair's spouse is cofounder, CEO, and has equity interest in Viewpoint Medical Inc. Andrew Kummel and William Trogler are scientific advisors/scientific cofounders and have an equity interest in Viewpoint Medical Inc. The terms of this arrangement have been reviewed and approved by the University of California, San Diego in accordance with its conflict of interest policies.

Keywords

glioblastoma, immunotherapy, nanoparticles, programmed cell death 1, ultrasound

Received: May 13, 2019
Revised: July 18, 2019
Published online: August 16, 2019

[1] J. Zeng, A. P. See, J. Phallen, C. M. Jackson, Z. Belcaid, J. Ruzevick, N. Durham, C. Meyer, T. J. Harris, E. Albesiano, *Int. J. Radiat. Oncol. Biol. Phys.* **2013**, *86*, 343.

[2] a) M. Preusser, M. Lim, D. A. Hafler, D. A. Reardon, J. H. Sampson, *Nat. Rev. Neurol.* **2015**, *11*, 504; b) Q. T. Ostrom, H. Gittleman, P. Liao, C. Rouse, Y. Chen, J. Dowling, Y. Wolinsky, C. Kruchko, J. Barnholtz-Sloan, *Neuro. Oncol.* **2014**, *16*, iv1.

[3] M. A. Curran, W. Montalvo, H. Yagita, J. P. Allison, *Proc. Natl. Acad. Sci. USA* **2010**, *107*, 4275.

[4] a) J. Duraiswamy, K. M. Kaluza, G. J. Freeman, G. Coukos, *Cancer Res.* **2013**, *73*, 3591; b) R. V. Parry, J. M. Chemnitz, K. A. Frauwirth, A. R. Lanfranco, I. Braunstein, S. V. Kobayashi, P. S. Linsley, C. B. Thompson, J. L. Riley, *Mol. Cell. Biol.* **2005**, *25*, 9543; c) O. Hamid, C. Robert, A. Daud, F. S. Hodi, W.-J. Hwu, R. Kefford, J. D. Wolchok, P. Hersey, R. W. Joseph, J. S. Weber, *N. Engl. J. Med.* **2013**, *369*, 134; d) S. L. Topalian, F. S. Hodi, J. R. Brahmer, S. N. Gettinger, D. C. Smith, D. F. McDermott, J. D. Powderly, R. D. Carvajal, J. A. Sosman, M. B. Atkins, *N. Engl. J. Med.* **2012**, *366*, 2443; e) R. L. Ferris, G. Blumenschein Jr, J. Fayette, J. Guigay, A. D. Colevas, L. Licitra, K. Harrington, S. Kasper, E. E. Vokes, C. Even, *N. Engl. J. Med.* **2016**, *375*, 1856.

[5] M. Lim, Y. Xia, C. Bettegowda, M. Weller, *Nat. Rev. Clin. Oncol.* **2018**, *15*, 422.

[6] A. C. Filley, M. Henriquez, M. Dey, *Oncotarget* **2017**, *8*, 91779.

[7] a) J. C. Bell, C. S. Ilkow, *Cancer Cell* **2017**, *32*, 133; b) N. A. P. Lieberman, K. DeGolier, H. M. Kovar, A. Davis, V. Hoglund, J. Stevens, C. Winter, G. Deutsch, S. N. Furlan, N. A. Vitanza, S. E. S. Leary, C. A. Crane, *Neuro-Oncology* **2019**, *21*, 83.

[8] K. Ni, G. Lan, C. Chan, B. Quigley, K. Lu, T. Aung, N. Guo, P. La Riviere, R. R. Weichselbaum, W. Lin, *Nat. Commun.* **2018**, *9*, 2351.

[9] J. Thariat, J.-M. Hannoun-Levi, A. Sun Myint, T. Vuong, J.-P. Gérard, *Nat. Rev. Clin. Oncol.* **2012**, *10*, 52.

[10] a) C. He, X. Duan, N. Guo, C. Chan, C. Poon, R. R. Weichselbaum, W. Lin, *Nat. Commun.* **2016**, *7*, 12499; b) X. Duan, C. Chan, N. Guo, W. Han, R. R. Weichselbaum, W. Lin, *J. Am. Chem. Soc.* **2016**, *138*, 16686; c) J. Xu, L. Xu, C. Wang, R. Yang, Q. Zhuang, X. Han, Z. Dong, W. Zhu, R. Peng, Z. Liu, *ACS Nano* **2017**, *11*, 4463; d) F. Hu, Y. Zhang, G. Chen, C. Li, Q. Wang, *Small* **2015**, *11*, 985.

[11] S. Stolik, J. A. Delgado, A. Pérez, L. Anasagasti, *J. Photochem. Photobiol., B* **2000**, *57*, 90.

[12] a) X. Hao, C. Li, Y. Zhang, H. Wang, G. Chen, M. Wang, Q. Wang, *Adv. Mater.* **2018**, *30*, 1804437; b) W. Zou, J. D. Wolchok, L. Chen, *Sci. Transl. Med.* **2016**, *8*, 328rv4.

[13] a) F. Orsi, L. Zhang, P. Arnone, G. Orgera, G. Bonomo, P. D. Vigna, L. Monfardini, K. Zhou, W. Chen, Z. Wang, *Am. J. Roentgenol.* **2010**, *195*, W245; b) F. Wu, Z.-B. Wang, Y.-D. Cao, W. Chen, J. Bai, J. Zou, H. Zhu, *Br. J. Cancer* **2003**, *89*, 2227.

[14] R. J. E. van den Bijgaart, D. C. Eikelenboom, M. Hoogenboom, J. J. Fütterer, M. H. den Brok, G. J. Adema, *Cancer Immunol. Immunother.* **2017**, *66*, 247.

[15] M. Hoogenboom, D. Eikelenboom, M. H. den Brok, A. Veltien, M. Wassink, P. Wesseling, E. Dumont, J. J. Fütterer, G. J. Adema, A. Heerschap, *NMR Biomed.* **2016**, *29*, 721.

[16] Y. Xing, X. Lu, E. C. Pua, P. Zhong, *Biochem. Biophys. Res. Commun.* **2008**, *375*, 645.

[17] A. Liberman, Z. Wu, C. V. Barback, R. D. Viveros, J. Wang, L. G. Ellies, R. F. Mattrey, W. C. Trogler, A. C. Kummel, S. L. Blair, *J. Surg. Res.* **2014**, *190*, 391.

[18] R. Stupp, W. P. Mason, M. J. Van Den Bent, M. Weller, B. Fisher, M. J. Taphoorn, K. Belanger, A. A. Brandes, C. Marosi, U. Bogdahn, *N. Engl. J. Med.* **2005**, *352*, 987.

[19] F. Forsberg, D. A. Merton, J. B. Liu, L. Needleman, B. B. Goldberg, *Ultrasonics* **1998**, *36*, 695.

[20] V. Pirro, C. M. Alfaro, A. K. Jarmusch, E. M. Hattab, A. A. Cohen-Gadol, R. G. Cooks, *Proc. Natl. Acad. Sci. USA* **2017**, *114*, 6700.

[21] G. Iacob, E. B. Dinca, *J. Med. Life* **2009**, *2*, 386.

[22] a) Z. Huang, L. Cheng, O. A. Guryanova, Q. Wu, S. Bao, *Protein Cell* **2010**, *1*, 638; b) M. Lara-Velazquez, R. Al-Kharboosh, S. Jeanneret, C. Vazquez-Ramos, D. Mahato, D. Tavanaiepour, G. Rahmathulla, A. Quinones-Hinojosa, *Brain Sci.* **2017**, *7*, 166.

[23] T. Selbekk, A. S. Jakola, O. Solheim, T. F. Johansen, F. Lindseth, I. Reinertsen, G. Unsgård, *Acta Neurochir.* **2013**, *155*, 973.

[24] A. Liberman, J. Wang, N. Lu, R. D. Viveros, C. Allen, R. Mattrey, S. Blair, W. Trogler, M. Kim, A. Kummel, *Adv. Funct. Mater.* **2015**, *25*, 4049.

[25] C. H. Huang, J. Wang, J. Yang, J. P. Oviedo, S. Nam, W. C. Trogler, S. L. Blair, M. J. Kim, A. C. Kummel, *Adv. Funct. Mater.* **2019**, p. 1900893.

[26] a) M. L. Fabiilli, K. J. Haworth, N. H. Fakhri, O. D. Kripfgans, P. L. Carson, J. B. Fowlkes, *IEEE Trans. Ultrason. Eng.* **2009**, *56*, 1006; b) O. Shpak, M. Verweij, H. J. Vos, N. de Jong, D. Lohse, M. Versluis, *Proc. Natl. Acad. Sci. USA* **2014**, *111*, 1697.

[27] O. D. Kripfgans, J. B. Fowlkes, D. L. Miller, O. P. Eldevik, P. L. Carson, *Ultrasound Med. Biol.* **2000**, *26*, 1177.

[28] H. Chen, X. Li, M. Wan, *Ultrason. Sonochem.* **2006**, *13*, 480.

[29] A. Liberman, Z. Wu, C. V. Barback, R. Viveros, S. L. Blair, L. G. Ellies, D. R. Vera, R. F. Mattrey, A. C. Kummel, W. C. Trogler, *ACS Nano* **2013**, *7*, 6367.

[30] E. Maloney, J. H. Hwang, *Int. J. Hyperthermia* **2015**, *31*, 302.

[31] J. MacDonell, N. Patel, S. Rubino, G. Ghoshal, G. Fischer, E. C. Burdette, R. Hwang, J. G. Pilitsis, *Neurosurg. Focus* **2018**, *44*, E11.

[32] D. L. Miller, J. Song, *Ultrasound in Medicine & Biology* **2002**, *28*, 1343.

[33] S. Nawaz, A. Heindl, K. Koelble, Y. Yuan, *Mod. Pathol.* **2015**, *28*, 766.

[34] R. Chetty, K. Gatter, *J. Pathol.* **1994**, *173*, 303.

[35] a) M. Zhang, S. Kleber, M. Röhrich, C. Timke, N. Han, J. Tuettenberg, A. Martin-Villalba, J. Debus, P. Peschke, U. Wirkner, M. Lahn, P. E. Huber, *Cancer Res.* **2011**, *71*, 7155; b) Y. Ma, Z. Cheng, J. Liu, L.

 © 2019 WILEY-VCH Verlag GmbH & Co. KGaA, Weinheim

Torre-Healy, J. D. Lathia, I. Nakano, Y. Guo, R. C. Thompson, M. L. Freeman, J. Wang, *Stem Cell Rep.* **2017**, *9*, 1948.
[36] a) K. K. Velpula, A. Bhasin, S. Asuthkar, A. J. Tsung, *Cancer Res.* **2013**, *73*, 7277; b) C. Zhan, B. Gu, C. Xie, J. Li, Y. Liu, W. Lu, *J. Controlled Release* **2010**, *143*, 136.
[37] J. G. Altin, E. K. Sloan, *Immunol. Cell Biol.* **1997**, *75*, 430.
[38] A.-K. Eerola, Y. Soini, P. Pääkkö, *Clin. Cancer Res.* **2000**, *6*, 1875.
[39] Y. Watanabe, K. Kuribayashi, S. Miyatake, K. Nishihara, E. Nakayama, T. Taniyama, T. Sakata, *Proc. Natl. Acad. Sci. USA* **1989**, *86*, 9456.
[40] C. Dostert, V. Pétrilli, R. Van Bruggen, C. Steele, B. T. Mossman, J. Tschopp, *Science* **2008**, *320*, 674.
[41] F. Ghiringhelli, L. Apetoh, A. Tesniere, L. Aymeric, Y. Ma, C. Ortiz, K. Vermaelen, T. Panaretakis, G. Mignot, E. Ullrich, J.-L. Perfettini, F. Schlemmer, E. Tasdemir, M. Uhl, P. Génin, A. Civas, B. Ryffel, J. Kanellopoulos, J. Tschopp, F. André, R. Lidereau, N. M. McLaughlin, N. M. Haynes, M. J. Smyth, G. Kroemer, L. Zitvogel, *Nat. Med.* **2009**, *15*, 1170.
[42] J. Deng, Y. Zhang, J. Feng, F. Wu, *Ultrasound Med. Biol.* **2010**, *36*, 441.
[43] F. Jolesz, G. T. Clement, N. McDannold, P. Black, K. Hynynen, *Neurosurgery* **2010**, *66*, 323.
[44] P. F. Bousquet, M. F. Braña, D. Conlon, K. M. Fitzgerald, D. Perron, C. Cocchiaro, R. Miller, M. Moran, J. George, X.-D. Qian, *Cancer Res.* **1995**, *55*, 1176.

 © 2019 WILEY-VCH Verlag GmbH & Co. KGaA, Weinheim